LUND UNIVERSITY

Tool–chip thermal conductance coefficient and heat flux in machining

Theory, model and experiment

Kryzhanivskyy, V.; Saoubi, R. M'; Ståhl, J. E.; Bushlya, V.

Link to publication

Manuscript draft

Title: Tool–chip thermal conductance coefficient and heat flux in machining: Theory, model and experiment

Article type: Research Paper

Abstract: This study proposes a technique for determining a tool–chip thermal conductance coefficient and heat flux in machining. The technique is based on solving an inverse heat transfer problem (IHTP). Because the IHTP is ill-posed, a priori information is required for its effective solution. To derive this information, substantial qualitative and quantitative analysis of a mixed boundary value problem for the heat equation and an illustrative test case for IHTP are provided. It has been established that the averaged interfacial chip temperature is needed for an effective IHTP solution. Thermal imaging combined with a special experimental setup was used to determine chip temperature. It was also found that a function describing the heat flux time dependency belongs to a set of decreasing functions. Tool–chip thermal conductance coefficients were obtained for high-speed steel and cemented carbide tooling. On the microscale, this data was interpreted in terms of a conforming rough surface contact conductance model, where tool wear was found to govern variations in the thermal conductance coefficient.

Keywords: Machining; Tool–chip thermal conductance coefficient; Heat flux; Inverse method

Taxonomy: Conventional Metal Cutting

Corresponding Author: Vyacheslav Kryzhanivskyy

Corresponding Author's Institution: Zhytomyr State Technological University

Order of Authors: Vyacheslav Kryzhanivskyy, Rachid MSAOUBI, Jan Eric Ståhl, Volodymyr Bushlya

Tool–chip thermal conductance coefficient and heat flux in machining: Theory, model and experiment

V.Kryzhanivskyy[a,c], R.M'Saoubi[a], J.-E.Ståhl[b], V.Bushlya[b]

[a]R&D, Seco Tools AB, SE-73782 Fagersta, Sweden

[b]Division of Production and Materials Engineering, Lund University, Ole Römers väg 1, Lund, 22100, Box-118, Sweden

[c]Department of Software systems, Zhytomyr Polytechnic State University, Chudnivska 103, Zhytomyr, 10005, Ukraine

Abstract

This study proposes a technique for determining a tool–chip thermal conductance coefficient and heat flux in machining. The technique is based on solving an inverse heat transfer problem (IHTP). Because the IHTP is ill-posed, a priori information is required for its effective solution. To derive this information, substantial qualitative and quantitative analysis of a mixed boundary value problem for the heat equation and an illustrative test case for IHTP are provided. It has been established that the averaged interfacial chip temperature is needed for an effective IHTP solution. Thermal imaging combined with a special experimental setup was used to determine chip temperature. It was also found that a function describing the heat flux time dependency belongs to a set of decreasing functions.

Tool–chip thermal conductance coefficients were obtained for high-speed steel and cemented carbide tooling. On the microscale, this data was interpreted in terms of a conforming rough surface contact conductance model, where tool wear was found to govern variations in the thermal conductance coefficient.

Keywords:

Machining; Tool–chip thermal conductance coefficient; Heat flux; Inverse method.

Nomenclature

ρ – Density, (kg/m^3)
c_p – Specific heat, J/(kg K)
k – Thermal conductivity, W/(m K)
t – Time, s
u – Temperature, ^{o}C
u_0 – Initial temperature, ^{o}C
$q, q(t)$ – Heat flux, W/mm^2
h – Coefficient of heat exchange with the environment, W/(mm^2 K)
h_{tcc} – Tool–chip thermal contact conductance coefficient, W/(mm^2 K)
u_{chip} – Average chip temperature, ^{o}C
u_{ext} – Temperature of the environment, ^{o}C
n – Outward normal to boundary
S – Tool surface

S_1 – Tool–chip interface
TC1, …, TC8 – Labels for thermocouples
m – Number of thermocouples
$u_i^{meas}(t), u_i^{calc}(t)$ – Measured and calculated temperature, respectively, at the position of i-th thermocouple installation, ^{o}C
T – Modeling time, s
H_C – Contact microhardness, MPa
P – Contact pressure, MPa
n – Contact spot density, items/m^2
a – Microcontact spot radius, m
k_{eff} – Effective thermal conductivity of the joint
$\psi(\varepsilon)$ – Thermal constriction parameter

1. Introduction

Although the temperature distribution in a cutting tool body is a by-product of the cutting process, it is important because it has a direct impact on the effectiveness and accuracy of the machining process [1]. Significant effort has thus been invested in obtaining reliable computational methods to determine the temperature distribution in a tool [2] as the fact that the temperature field is a three-dimensional distributed characteristic limits the use of direct experimental measurements.

The basis of computational methods is the heat transfer equation, the essence of which is the differential formulation of the energy conservation law in the neighborhood of any internal point of the body. There are no fundamental difficulties in its solution once the boundary conditions are known. However, this presents an interesting problem: Do Dirichlet, Neumann, or mixed boundary conditions most closely describe the case to be modeled? How should the physical parameters be determined with acceptable accuracy? These questions become more complicated because the most important thermophysical part of the boundary — the tool–chip contact — is extremely small compared to the rest of the tool surface.

This issue has led to the creation of hybrid models that take into account both the macroscale tool heat transfer and microscale machining mechanics in order to reconstruct the 3D tool temperature field [3]. In this context, the consistency of the macro- and micromodels is important to consider. First, the heat balance has to be determined on a macroscale in average, resulting from the condition of energy conservation. This heat balance determines the average characteristics for the micromodel. And then on a microscale, the heat has to be redistributed in time and space taking into account surface topography and interaction conditions.

It is known that almost all the power consumed during metal cutting is converted into heat [4]. Therefore, the total amount of heat distributed between tool, chip, workpiece, and environment can be easily calculated as the product of the cutting force and the cutting speed. To determine the heat distribution, researchers have studied heat fluxes into the tool, chip and workpiece. A number of papers have been devoted to heat flux determination in different machining processes such as deep grinding [5], high-speed drilling [7], dry machining of aeronautic aluminum alloy [9], MQL tapping and reaming [10] or devoted to prediction of heat flux distribution [6] and its effect on tool thermal deformation [8]. On the one hand, heat flux is the boundary condition (initial data) for the heat transfer equation, and on the other hand, it is a parameter that is almost impossible to measure due to the small area of the tool–chip contact and the aggressiveness of the cutting process. Thus the inverse heat conduction problem has become one of the main instruments for calculating the heat flux [11]. The solution of this problem gives rise to various techniques, let's say, modal approach [12], sequential algorithm [18], selection method [16], or curve fitting for heat flux time dependency [17], as well as to developing of temperature data collection methods such as thin film thermocouples measurement [15], infrared camera [19], or embedded temperature measuring tool holder system [20].

However, inverse problems are ill-posed [22] and therefore their solution methods are very sensitive to the accuracy of the initial data and can return solutions that do not correspond to the physics of the cutting process [13, 14]. Thus it is very important to have accurate a priori information about the phenomenon being investigated [23]. To illustrate the importance, it should be noted that the ill-posedness of inverse heat transfer problem requires a regularization mechanism in the solution method. Its role is to suppress the "wrong" or "parasitic" solutions of the inverse problem. This mechanism is formed on the basis of additional, a priori information on the solution. Existing, relatively universal methods for solving the inverse heat transfer problem use smoothness as a regularization, because parasitic solutions very often are highly oscillating functions. In numerical methods, such a regularization penalizes sharp changes in the sought function. In this case, if the function really had a segment with a sharp, for example, decreasing character (Fig. 15) then it would not be restored correctly. For

3

instance, reported in [13], the time dependency of the heat flux demonstrates relatively slow increasing and decreasing trends during tool engagement and disengagement. This fact is inconsistent with reality, because, for example, the flux becomes zero practically instantly when tool disengaged. In [13, Page 1645], the problems of the solution methods are honestly mentioned "These methods deform the shape of the estimated heat flux versus time diagram especially in the regions that the heat flux changes sharply (the start and the end of machining)". Returning to the sense of the regularization as an additional information on the solution behavior, this information provides a mechanism for the formulation of a set of feasible solutions that correspond to the physics of the process.

On the basis of the recommendations of [24] and [1], an experimental setup was proposed to ensure high accuracy of the initial data on the temperatures in the tool body. The experiments showed that the time dependency of heat flux into tool is described by a decreasing function [21], thus creating a description of a priori behavior. However, the exact shape of the decreasing trend, which is currently approximated by a power function, remains unknown. Similarly, questions remain about how the conditions of the machining process govern the functional behavior of the heat flux and how this behavior reflects the thermal phenomena in the cutting zone.

In [21] the Neumann condition (heat flux dependent on time) was used as the boundary condition for the heat equation. The function describing the time dependency of the heat flux was considered as unknown and was chosen from a set of decreasing functions. The argument for choosing a function that decreases over time was that the maximum intensity of the flux occurs at first contact, when the practically cool tool meets the chip temperature at the interface, and flux is proportional to the temperature difference. As the tool heats up, the heat flux drops rapidly at first, and then decreases at a slower rate. On the other hand, the limiting case of this reasoning is the explicit assignment of the temperature (chip) at the tool boundary, which, under constant cutting conditions, remains unchanged during machining. In terms of boundary conditions, this is the Dirichlet boundary condition [25]. So the question is, which approach should be preferred: the assignment of the temperature (Dirichlet condition), or the heat flux across the tool boundary (Neumann condition).

A compromise in this case is the mixed boundary condition of the form:

$$-k\frac{\partial u}{\partial n} = h_{tcc}(u - u_{chip}), \qquad\qquad (1)$$

where h_{tcc} is the tool–chip thermal contact conductance coefficient.

This equation summarizes both the Dirichlet and Neumann conditions, because when h_{tcc} tends to infinity, the temperature equals the chip temperature (the Dirichlet condition). On the other hand, with smaller values of h_{tcc}, all possible intermediate heat flux values are stipulated down to zero (the Neumann condition). Another advantage of using the mixed boundary condition is that the coefficient h_{tcc} characterizes the thermal conductance of the tool–chip contact interface [26, 29]. The importance of this coefficient for adequate thermal modeling of the cutting process can be seen by the number of publications on this subject which consider coefficient h_{tcc} in view of friction [27, 30] or thermal contact resistance [28].

This paper uses the same temperature data set as the previous research that relied on the Neumann boundary condition [21]. However, in this paper the analysis uses the mixed boundary condition (Eq. 1), and the time dependence of the heat flux is not regulated a priori but depends on the coefficient h and can be numerically determined as a result of the simulation. Finding this coefficient will answer the question about the exact form of the heat flux time dependency and link it to the cutting process parameter (thermal resistance at the tool–chip interface). It will also evaluate the accuracy of the approximation of the exact form of the heat flux with the help of the power function from [21].

2. Boundary condition analysis

2.1 Boundary value problem

As stated in the introduction, when formulating a boundary value problem the most important aspect is the adequate formulation of boundary conditions. This is because the role of the heat equation is only to represent the energy conservation law in the neighborhood of interior points within a tool body. Given that a tool itself is an assembly of multiple components, it is also important to establish the correct description of thermal contacts between them.

Because heat transfer inverse problems are very sensitive to the accuracy of the measurement data [11], the authors earlier proposed [17, 21] an experimental setup to obtain temperatures in a cutting tool so that the uncertainties are minimized. The uncertainties that remain are analyzed from the point of view of their influence on the result. This allows accurate data on temperatures within a tool body to be obtained [21]. In those papers, the inverse heat conduction problem was used with the temperature distribution described by the Neumann boundary value problem:

$$div(k(u)grad\ u) = \rho c_p(u)\frac{\partial u}{\partial t} \tag{2}$$

$$k(u)\frac{\partial u}{\partial n}\bigg|_{S_1} = q(t) \tag{3}$$

$$-k(u)\frac{\partial u}{\partial n}\bigg|_{S \backslash S_1} = h(u - u_{ext}) \tag{4}$$

$$u|_{t=0} = u_0. \tag{5}$$

This formulation assigns the temperature distribution in a body to an unknown heat flux $q(t)$ flowing into a tool through a tool–chip interface (Fig. 1). Additional complexity might be introduced if the heat flux has a spatial resolution, $(q(x,t))$. However, the experimental setup was designed [21] to minimize the impact of spatial resolution while maximizing time resolution. Thus, the flux spatial distribution is considered uniform.

The boundary condition (Eq. 3) also does not reflect the cause of the heat flux. It is known [4] that nearly all the power consumed in a machining process is converted to heat and results in a chip temperature u_{chip}. If spatial distribution is neglected, the heat flux is assumed to be proportional to the temperature difference between the contacting pair, the tool and the chip (Fig. 1).

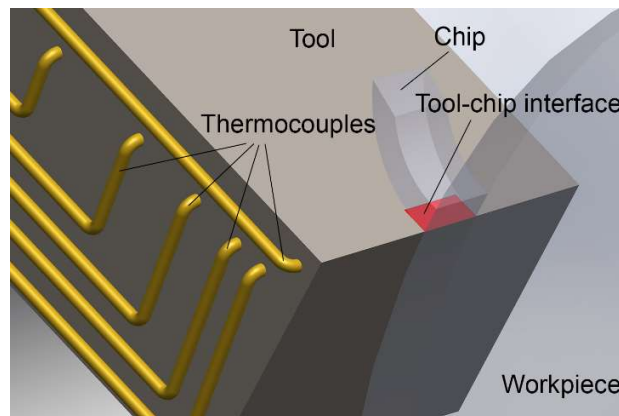Mathematically, this corresponds to the mixed boundary condition of Eq. 1.

Fig. 1. Schematic of tool–workpiece interaction including tool-chip interface and embedded thermocouples.

This choice of boundary condition makes it possible to include the chip temperature u_{chip} and heat conductance coefficient h_{tcc} in the solution of the problem (Eqs. 2, 4, and 5), thus characterizing the thermal conditions of the tool–chip interface.

2.2 Qualitative analysis of the boundary value problem solution

Equation (Eq. 2) is nonlinear because material thermophysical properties are temperature dependent. Analyzing the functional behavior of nonlinear problem solutions requires the use of complex methods of functional analysis and a detailed description of the nature of the nonlinearity [31]. In our case, the dependence of material properties on the temperature within the range of interest is relatively weak and is described by smooth bounded functions [21]. Therefore, for *qualitative* analysis, the problem (Eq. 1, 2, 4, 5) can be linearized. Thus the thermophysical properties are considered to be independent of temperature and equal to the average values within the temperature range. Detailed analysis of nonlinearity is not considered in this section and is restricted to the linear case of the problem (Eq. 1, 2, 4, 5).

The linearized heat conduction problem has the form:

$$\Delta u = \frac{\rho c_p}{k} \frac{\partial u}{\partial t}, \tag{6}$$

$$k \frac{\partial u}{\partial n} + h(x)u \Big|_S = h(x)\,\varphi(x), \tag{7}$$

$$u|_{t=0} = u_0, \tag{8}$$

where

$$\varphi(x) = \begin{cases} u_{ext}, & if\ x \in S \backslash S_1 \\ u_{chip}, & if\ x \in S_1 \end{cases},$$

$$h(x) = \begin{cases} h, & if\ x \in S \backslash S_1 \\ h_{tcc}, & if\ x \in S_1 \end{cases}.$$

The solution of the problem (Eq. 6–8) is defined unambiguously according to the existence and uniqueness theorem [25]. However, this solution is a function that depends parametrically on the chip temperature u_{chip} and coefficient h_{tcc}.

The Fourier method is used to obtain a formal solution of the problem (Eq. 6–8). First the solution of the problem (Eq. 6–8) is presented as the sum

$$u = v + \omega, \tag{9}$$

where v is the solution of the problem with homogenous boundary conditions

$$\Delta v = \frac{\rho c_p}{k} \frac{\partial v}{\partial t}, \tag{10}$$

$$k \frac{\partial v}{\partial n} + hv \Big|_S = 0, \tag{11}$$

$$v|_{t=0} = u_0 - \omega \tag{12}$$

and ω is the solution of steady-state heat equation with non-homogenous boundary conditions

$$\Delta \omega = 0,\ k \frac{\partial \omega}{\partial n} + h(x)\omega \Big|_S = h(x)\,\varphi(x). \tag{13}$$

The formal solution of the problem (Eq. 10–12) can be written in the form [25]

$$v(x, t) = \sum_{k=1}^{\infty} a_k \exp(-\lambda_k t) W_k(x),$$ (14)

where

$$a_k = \frac{\rho c_p}{k} \int_G (u_0 - \omega) W_k(x) dx,$$

G is the tool body, $W_k(x), \lambda_k, k = 1, 2, \dots$ are eigenfunctions and eigenvalues of the problem (Eq. 10–12), respectively.

Let us consider the flux $q(x, t)$ through the surface S_1 as a function of t in the problem (Eq. 6–8)

$$q(x, t)|_{S_1} \triangleq -k \frac{\partial u}{\partial n}\bigg|_{S_1} = h_{tcc}(u - u_{chip}).$$ (15)

Now, taking into account (Eq. 9) and (Eq. 14), the following formula can be obtained:

$$q(x, t)|_{S_1} \triangleq h_{tcc}\left(\sum_{k=1}^{\infty} a_k \exp(-\lambda_k t) W_k(x) + \omega - u_{chip}\right).$$ (16)

Formula (Eq. 16) represents the heat flux as an eigenfunction expansion which parametrically depends on concrete parameters (chip temperature u_{chip} and coefficient h_{tcc}). However, using this formula would require the eigenvalues and functions in Eq. 15 to be found analytically for realistic tool geometries and assemblies as well, which is computationally prohibitive. On the other hand, it is known [4] that u_{chip} reaches its steady state temperature within the first second of tool engagement while the tool body remains practically cool. It corresponds to maximum intensity of the heat flux because it is proportional to the difference of temperatures [32]. Then the difference becomes smaller and continue to decrease as the tool is heated up. This implies that when solving a heat conduction inverse problem, the solution should be chosen from decreasing functions of t. A simple unidimensional case (section 3.1), which can be treated analytically, reveals the pattern for decreasing heat flux as well as the functional behavior of an inverse problem solution.

3. Analysis of heat transfer problem

As demonstrated above, there is physical justification for a decreasing heat flux function that depends on u_{chip} and h_{tcc} (Eq. 15, 16). Therefore, u_{chip} and h_{tcc} are the variables required to solve the heat conduction inverse problem. Since the efficiency of solving the inverse heat conduction problem depends on a priori information about the behavior of the solution, it is useful to study in detail the dependence of its solution on u_{chip} and h_{tcc}. To do this, a simplified boundary problem is considered as an illustrative test case, for which it is possible to obtain an analytical solution relatively easily.

3.1. One-dimensional illustrative test case

In this section, the bar-shaped test body shown in Fig. 2 is used to illustrate the Fourier method for obtaining heat flux as an analytical function depending on h and external temperature u_{ext}.
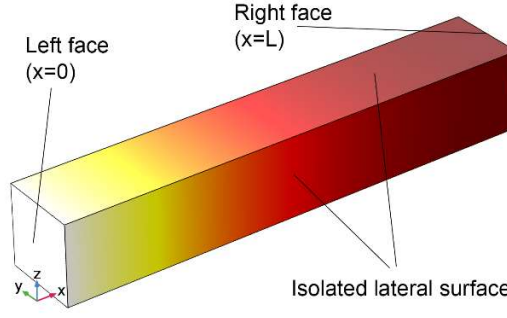
Fig. 2. Geometry of the test body for the heat conduction problem.

The bar is isolated on lateral surfaces, the mixed boundary condition is specified on the left face ($x = 0$) and the Neumann's condition on the right face ($x = L$) (Fig. 2). The temperature distribution in this body can be described using the one-dimensional boundary value problem for the heat equation:

$$\frac{\partial u}{\partial t} = \frac{k}{c_p \rho} \frac{\partial^2 u}{\partial x^2},$$
(17)

$$k \frac{\partial u}{\partial x}\bigg|_{x=0} = h(u - u_{ext}),$$
(18)

$$\frac{\partial u}{\partial x}\bigg|_{x=L} = 0,$$
(19)

$$u|_{t=0} = u_0.$$
(20)

To apply the Fourier method, Eq. 18 is re-formulated as follows

$$-k \frac{\partial u}{\partial x} + hu\bigg|_{x=0} = hu_{ext}$$

and a new function $v = u - u_{ext}$ is introduced to obtain homogeneous boundary conditions.

Now, the solution to the problem (Eqs. 17–20) is obtained by substituting the auxiliary function in Eq. 17:

$$\frac{\partial v}{\partial t} = \frac{k}{c_p \rho} \frac{\partial^2 v}{\partial x^2},$$
(21)

$$-k \frac{\partial v}{\partial x} + hv\bigg|_{x=0} = 0,$$
(22)

$$\frac{\partial v}{\partial x}\bigg|_{x=L} = 0,$$
(23)

$$v|_{t=0} = u_0 - u_{ext}.$$
(24)

Now the solution of the problem (Eqs.21–24) can be presented in the form of a series

$$v(x,t) = \sum_{i=1}^{\infty} C_i \exp\left(-\frac{k}{c_p \rho} \lambda_i t\right) X_i(x),$$
(25)

where $X_i(x) = \frac{h}{k} \sin\left(\sqrt{\lambda_i} x\right) + \sqrt{\lambda_i} \cos\left(\sqrt{\lambda_i} x\right)$ and λ_i, $i = 1,2,\dots$ are eigenfunctions and eigenvalues.

The eigenvalues $\lambda_i, i = 1,2,\dots$ are determined from the following nonlinear equation

$$\sqrt{\lambda_i} = \frac{h}{k}\cot\left(\sqrt{\lambda_i}L\right).$$

The coefficients C_i are determined from the expansion by eigenfunctions $X_i(x)$ of the initial condition (Eq. 24).

$$u_0 - u_{ext} = \sum_{i=1}^{\infty} C_i\left(\frac{h}{k}\sin\left(\sqrt{\lambda_i}x\right) + \sqrt{\lambda_i}\cos\left(\sqrt{\lambda_i}x\right)\right), \tag{26}$$

where

$$C_i = \frac{\int_0^L (u_0 - u_{ext})\left(\frac{h}{k}\sin\left(\sqrt{\lambda_i}x\right) + \sqrt{\lambda_i}\cos\left(\sqrt{\lambda_i}x\right)\right)dx}{\int_0^L \left(\frac{h}{k}\sin\left(\sqrt{\lambda_i}x\right) + \sqrt{\lambda_i}\cos\left(\sqrt{\lambda_i}x\right)\right)^2 dx}. \tag{27}$$

Finally, the solution to Eqs. 21–24 is given by Eq. 25, where $C_i, i = 1,2,\dots$ have the form given in Eq. 27, and the solution to Eqs. 17–20 is accomplished easily by back substitution

$$u = u_{ext} + \sum_{i=1}^{\infty} C_i \exp\left(-\frac{k}{c_p\rho}\lambda_i t\right)\left(\frac{h}{k}\sin\left(\sqrt{\lambda_i}x\right) + \sqrt{\lambda_i}\cos\left(\sqrt{\lambda_i}x\right)\right).$$

This one-dimensional heat conduction test problem makes it possible to present the heat flux through the left face ($x = 0$) of the test body shown in Fig. 2 in an analytical form

$$Flux(t) = -k\left.\frac{\partial u}{\partial x}\right|_{x=0} = -k\sum_{i=1}^{\infty} C_i \exp\left(-\frac{k}{c_p\rho}\lambda_i t\right)\left(\frac{h}{k}\sqrt{\lambda_i}\cos\left(\sqrt{\lambda_i}x\right) - \lambda_i\sin\left(\sqrt{\lambda_i}x\right)\right)\Bigg|_{x=0} =$$

$$= -k\sum_{i=1}^{\infty} C_i \exp\left(-\frac{k}{c_p\rho}\lambda_i t\right)\left(\frac{h}{k}\sqrt{\lambda_i}\right) = -\sum_{i=1}^{\infty} C_i\left(h\sqrt{\lambda_i}\right)\exp\left(-\frac{k}{c_p\rho}\lambda_i t\right). \tag{28}$$

As a numerical example to show the heat flux time dependency, consider the case of heating a steel bar under the following conditions and properties: k = 44.5 W/(m K), ρ = 7850 kg/m³, c_p = 475 J/(kg K), L = 0.15 m, u_0 = 20 °C, u_{ext} = 500 °C, and T = 300 s. Fig. 3 shows the results for different values of h [W/m²K].
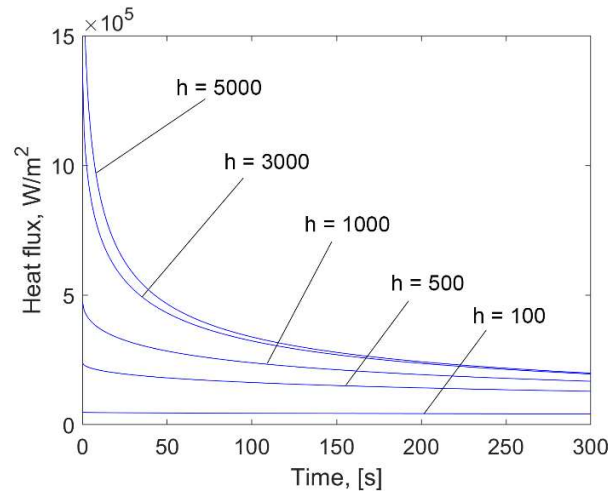

Fig. 3. Heat flux time dependency for different values of h.

The one-dimensional test case presented in this section serves three purposes:

1. Numerical illustration of *analytical heat flux determination* using the expansion by eigenfunctions of the boundary value problem (Eq. 28).

2. Visual inspection (Fig. 3) of *heat flux behavior* over time and its dependency on h.

3. Ability to identify *features of an inverse heat transfer problem* using the test case free of uncertainties related to measurements and numerical solution methods.

3.2. Features of the inverse heat conduction problem solution

From sections 2.1 and 2.2, it follows that as soon the boundary value problem is defined, the required parameters become the temperature of the chip u_{chip} and the heat transfer coefficient h_{tcc} between the hot chip and the tool body that is being heated. The test example (Eqs. 17–20) makes it possible to investigate the influence of their equivalents u_{ext} and h on the solution of the test inverse problem. Consider the following test inverse heat conduction problem.

1. Consider the problem (Eqs. 17–20, Fig. 2) as having the same numerical parameters, except for $h = 2 \cdot 10^4 \, W/(m^2 K)$, $T = 100 \, sec$, and $u_{ext} = 430 \, °C$ (Fig. 4a).

2. Introduce control points (Fig. 4a) and calculate temperatures at these points (Fig. 4b). These data are treated as "measurement" data or "thermocouple" readings with absolute accuracy.

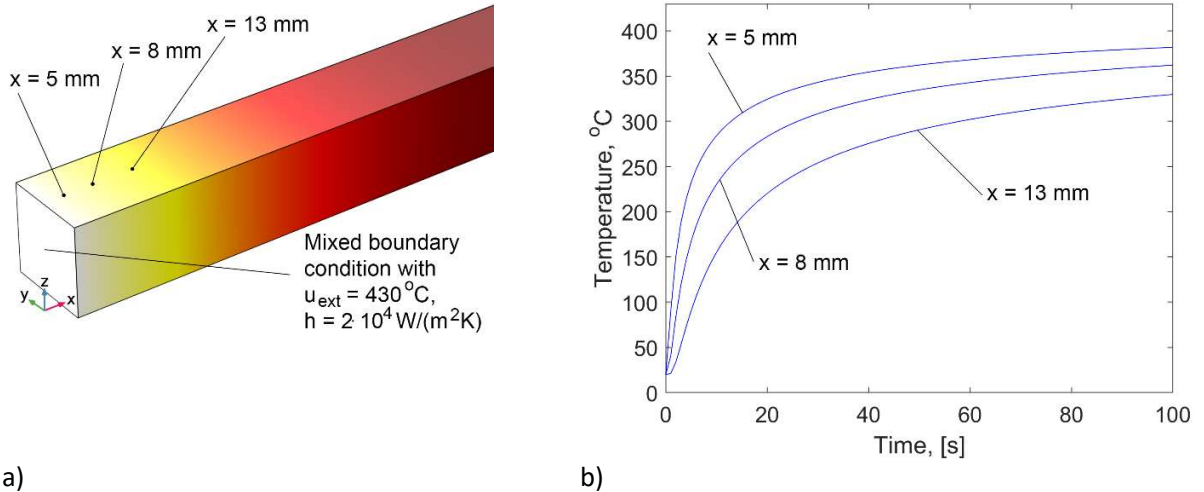a)   b)

Fig. 4. a) The positions of control points for temperature calculations; b) The temperature data at the given points.

3. Specify the objective function [21] which evaluates the deviation from the "measurement" data, when u_{ext} and h are changing (Eq. 29).

$$f(u_{ext}, h) = \frac{1}{\sqrt{T}} \sqrt{\int_0^T \left(\sum_{i=1}^3 u_i^{calc}(t) - u_i^{meas}(t) \right)^2 dt} \to min \qquad (29)$$

This is the optimization problem whose solution ($h = 2 \cdot 10^4 \, W/(m^2 K)$ and $u_{ext} = 430 \, °C$) is known.

To inspect the objective function behavior, consider its response surface shown in Fig. 5a and contour lines (Fig. 5b).

a)   b)
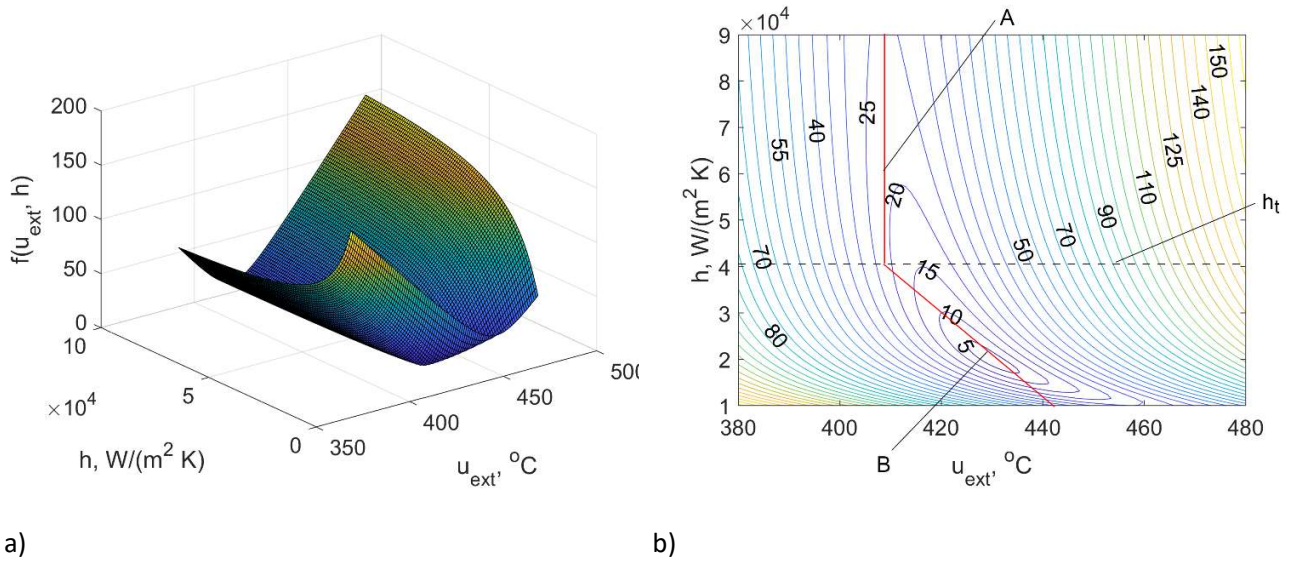
Fig. 5. a) The narrow curved valley of the objective function; b) Contours of the objective function (Eq. 29).

Fig. 5 shows that the objective function is a narrow curved valley that contains the minimum. Of course, in an ideal case, it is easy to find the minimum of such a unimodal function using an optimization algorithm that takes into account the narrow valley, and thus solve the inverse heat conduction problem. Moreover, as soon as one realizes that the solution depends only on the *parameters* u_{ext}, h and not on the *functions*, the inverse problem becomes well-posed [33].

One can note that Fig. 5b illustrates the fact that, starting from a certain threshold h_t (Fig. 5b), the value of the objective function becomes practically independent of h and depends only on u_{ext} (as the contours of the objective are almost parallel to the axis h). Such a value h_t corresponds to the actual transformation of the mixed boundary condition into the Dirichlet boundary condition, as mentioned in the introduction.

Using this threshold, the narrow valley can be roughly divided into two sections, A and B, above and below threshold (Fig. 5b). In practical cases, due to the limited accuracy of measured temperatures, the optimization algorithm might converge to almost any point in the region of the narrow valley bottom. This leads to two types of errors when solving the inverse heat conduction problem.

In the first case, when the algorithm converges to a point in section B, the overestimated real temperature value u_{ext} is "compensated" for by the underestimated value of h and vice versa. For a mathematical algorithm solving the optimization problem, these two variables u_{ext} and h are completely independent. If the algorithm can improve the objective function by making such a compensation it will of course do so. This is especially true for measured temperature data that always has unavoidable noise.

In the second case (section A), an underestimated u_{ext} temperature value can lead to completely inadequate large values of h. This is because the mixed boundary condition becomes equivalent to the Dirichlet condition, and the temperature field in the tool is controlled only by the temperature u_{ext}.

The existence of these two cases (sections A and B) means that for a correct solution of the inverse problem h and u_{ext} cannot be treated as two independent variables. It is absolutely necessary to resolve one of them, or at least estimate its value. It is experimentally easier to do so for temperature u_{ext}, because u_{ext} in the case of machining corresponds to an average chip temperature.

Another important observation that should be made from the analysis of Fig. 5 is that, due to the pronounced curvature of the narrow valley and its asymmetric shape, overestimation of the chip temperature results in a smaller error when determining h than underestimation of u_{ext}. For example, for the illustrative test case (Fig. 4), if the temperature u_{ext} is intentionally fixed at the value of 440 °C (overestimation by 10 °C) the objective function returns $h = 2.5 \cdot 10^4 \, W/(m^2 K)$ (error of 0.5·10⁴ W/m²K). Yet, for the temperature fixed at 420 °C (underestimation by 10 °C) the value of $h = 1 \cdot 10^4 \, W/(m^2 K)$ is returned (error of 1·10⁴ W/m²K).

3.3 The technique for numerically determining the time dependency of the heat flux into the tool

Section 2.2 showed that the time dependency of the heat flux in a tool cannot be obtained as a function of h and u_{chip} in an explicit analytical form, due to unresolvable geometric complexities for which there are no analytical eigenfunctions $W_k(x), k = 1,2, \ldots$ (Eq. 14). Practically, however, the total number of Joules consumed by the tool [21] can be obtained numerically using commercial software such as COMSOL Multiphysics.

Fig. 6 illustrates this technique and its accuracy for the numerical example of the test case (Eqs. 17–20) when h = 1000 (W/m²K).
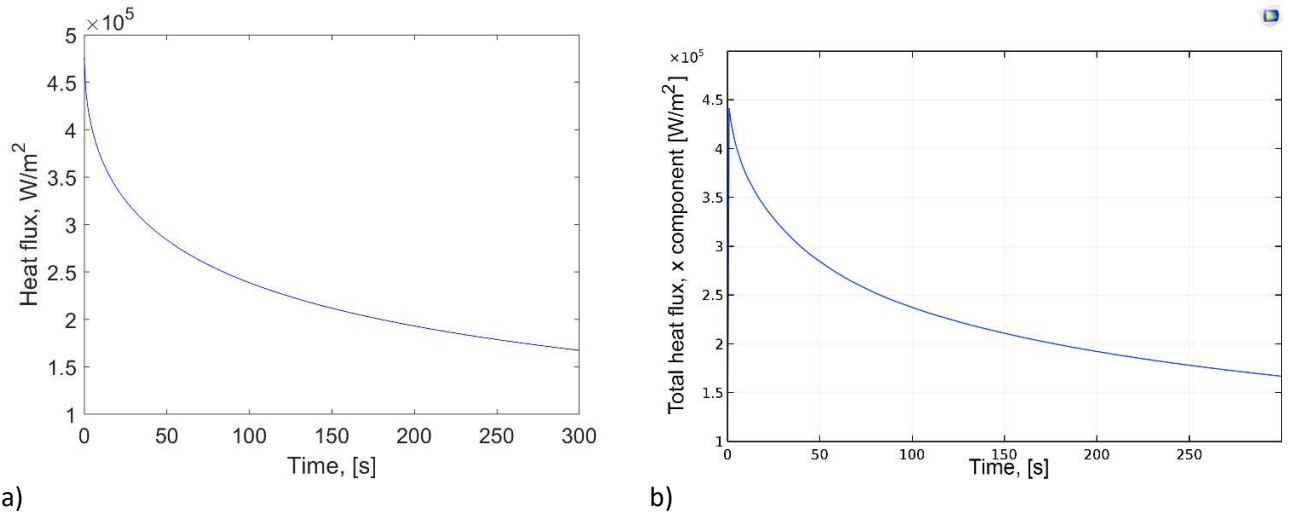

a)   b)

Fig. 6. a) Heat flux obtained analytically (Eq. 28); b) Heat flux obtained in COMSOL Multiphysics for identical test case.

Thus, when solving a realistic inverse problem, it is not necessary to select a predefined curve form for the heat flux time dependency as was done in [21] using only u_{chip} and h. As soon as the boundary problem is solved numerically, the time dependency of the heat flux can be back calculated from the numerical solution, also in a numerical form. But here it should be noted that the numerical solution can yields artefacts absent in the actual solution. For example, in Fig. 6b there is a sharp increasing component in the beginning of the curve which is absent in the analytical solution (Fig. 6a). Therefore the results of numerical modelling need to be examined from the point of view of mathematical physics.

3.4 Summary of analysis

1. The time dependency of the heat flux is a decreasing (non-increasing) function parametrically dependent on u_{chip} and h_{tcc}.
2. The inverse heat transfer problem cannot be effectively solved when u_{chip} and h_{tcc} are considered as two independent variables.

3. In a realistic case, the solution of the boundary value problem (Eqs. 1, 2, 4, 5) is obtained numerically as soon as u_{chip} and h_{tcc} have been found. Then the time dependency of the heat flux can be calculated from this numerical solution.

Consequently, the following strategy can be proposed for solving the inverse problem.

1. Determine the chip temperature u_{chip} using a specially designed experimental setup based on IR thermography measurements or another technique capable of returning interfacial chip temperature.
2. Provide a FE model for the mixed boundary value problem for the heat transfer equation (Eqs. 1, 2, 4, 5) which has h_{tcc} as an unknown parameter (a variable in an inverse heat transfer problem).
3. Solve the resulting inverse heat transfer problem using the temperature measurements at the control points (e.g. thermocouple readings taken from [21]).
4. Retrieve the heat flux time dependency numerically from the numerical solution of the problem (Eqs. 1, 2, 4, 5).

4. Inverse heat conduction problem solution

4.1 Chip temperature measurement

The chip temperature was measured during orthogonal cutting of the disk using the thermography technique [34]. The setup was designed to reproduce the cutting conditions of study [21] for the tests denoted as HSS2 and CC1 (Table 1). The manufactured inserts with zero rake angle and a flank angle of 7° were mounted in a specially adapted commercial toolholder CFIL3225P05. The insert materials were identical to those used in [21]. Fig. 7 illustrates the experimental setup.

Table 1. Test conditions.

Experiment acronym	Cutting conditions		Materials	
	Cutting speed, m/min	Feed, mm/rev	Workpiece	Insert
HSS2	300	0.15	Aluminum 5754	High-speed steel
CC1	100	0.05	Steel EN S235JR	Cemented Carbide

A thermal imaging camera from the FLIR X6000sc Series was used for the thermography measurements. The camera featured a high-speed 640 × 512 digital InSb detector with broadband (1.5–5.5μm) spectral sensitivity. It provided images up to 350 Hz in full frame, and it was calibrated up to 3000 °C with measurement accuracy of ± 1 °C. Short-duration tests (~6 s) were carried out, but the cutting time chosen was sufficient to reach a steady state interfacial chip temperature u_{chip}, because the average interfacial chip temperature is stabilized less than one second (Fig.9).
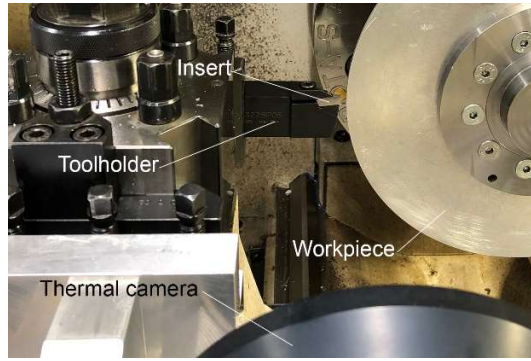
Fig. 7. Photograph of the experimental setup.

The interfacial chip temperature from the thermal imaging data was determined as follows. First, the interfacial chip temperature (Fig. 8) was measured for each frame along the line L with the length equal to the value of the contact length [21]. Second, the temperature was averaged over the experiment time (Fig. 9). To estimate the uncertainty in determining the average interfacial chip temperature, the standard deviation of the data was calculated (the dotted red line in Fig. 9). The emissivity values used in the experiments were 0.2 for steel [26] and 0.3 for oxidized aluminum [39].
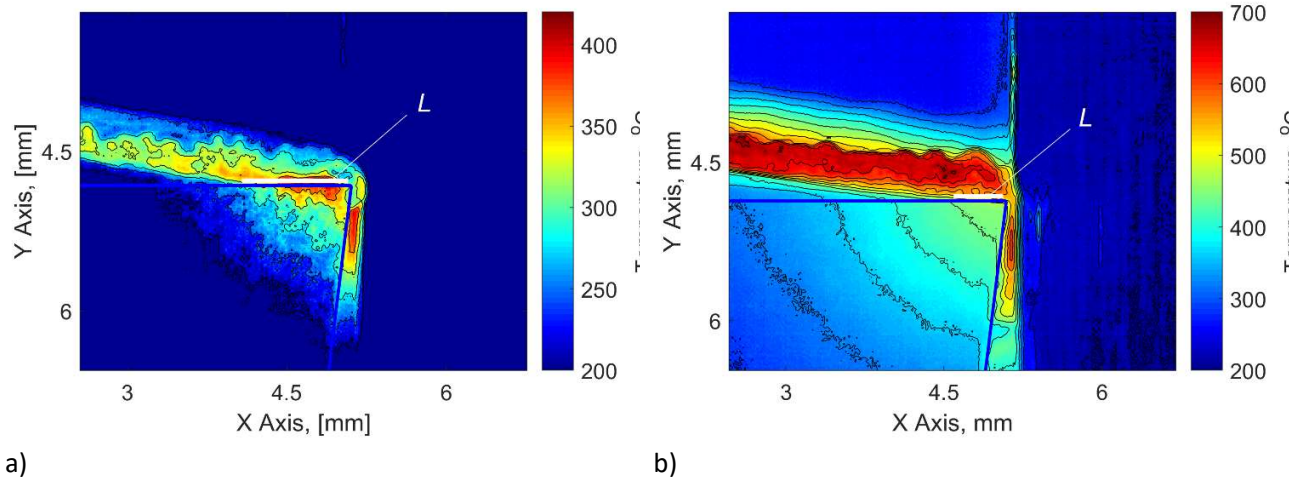

a)   b)

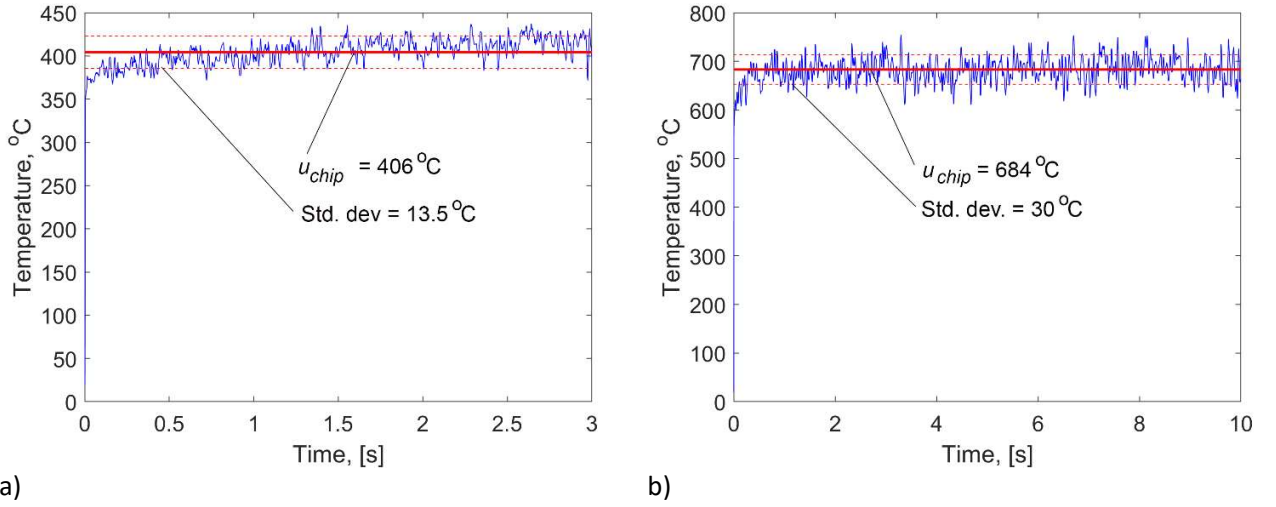Fig. 8. Typical thermal image for a frame: a) HSS2, b) CC1.

Fig. 9. The average interfacial chip temperature (blue line) along line L during the experiment for each frame, and the chip temperature averaged over time (red line): a) HSS2, b) CC1.

4.2 Inverse problem

In section 3, the average interfacial temperature of the chip u_{chip} in contact with the tool was determined. From the point of view of the objective function [21]

$$f(h_{tcc}) = \frac{1}{\sqrt{T}} \sqrt{\int_0^T \left(\sum_{i=1}^m u_i^{calc}(t) - u_i^{meas}(t) \right)^2 dt} \qquad (30)$$

which estimates the difference between measured and calculated temperatures, there is only one variable left, the coefficient h_{tcc}. The importance of studying this coefficient was noted in the introduction. It is known that the h_{tcc} value might not be uniform across the tool–chip interface and may have a particular spatial distribution [28]. It is also very likely that it is time dependent. The proposed setup for temperature measurement in the tool body [21] does not allow estimation of the spatial distribution of h_{tcc}. Therefore, the spatial distribution is assumed to be uniform, that is, an average heat exchange coefficient between the chip and the tool is returned by the inverse problem. However, its time resolution can be addressed with the existing experimental setup and measured data [21]. The thermocouple readings for h_{tcc} determination were also taken from [21].

h_{tcc} is assumed to be time dependent. This assumption creates additional computational difficulties because the inverse heat conduction problem becomes functional [33] and, as a result, ill-posed. Numerical methods for determining the unknown function $h_{tcc}(t)$ from the arsenal of existing algorithms [22] can lead to oscillations of the sought function as well as several other artifacts [21]. To avoid this, a two-stage method for solving the inverse heat conduction problem [21] can be used.

In the first stage, the problem is solved assuming that the coefficient h_{tcc} is time independent and constant. This solution will make it possible to evaluate the significance of the time dependency of the coefficient h_{tcc} and propose a suitable parameterized function based on this a priori information. The parameters of this function will be the variables of the inverse problem at the second stage.

4.2.1. Stage 1

The results of stage 1 for the HSS2 case (Table 1) are summarized in Table 2. Because there is an uncertainty in the average chip temperature (Fig. 9a), the calculations are performed for the upper and lower bounds of the chip temperature to estimate the uncertainty in h_{tcc} determination.

15

Table 2. h_{tcc} coefficient returned for the HSS2 case.

Chip temperature, °C	Coefficient h_{tcc}, W/(m² K)	Objective function, °C
406 (mean)	91077	1.5823
419.5 (upper bound, mean + std. dev.)	74286	1.5430
392.5 (lower bound, mean - std. dev.)	113965	1.5618

Very similar values of the objective function indicate the high agreement between the calculated and measured temperatures (Fig. 10a) in all the considered cases. This agreement reflects the fact that the proposed method for solving the inverse heat conduction problem compensates for the uncertainty in the chip temperature determination by an uncertainty in h_{tcc}, which is much larger in relative terms (Fig. 5). Also, the uncertainty in the definition of h_{tcc} has a pronounced asymmetry (Fig. 10b), even though the uncertainty of the chip temperature is symmetrical (Fig. 9.a). This is due to the behavior of the narrow valley of the objective function (Fig. 5) described in section 3.
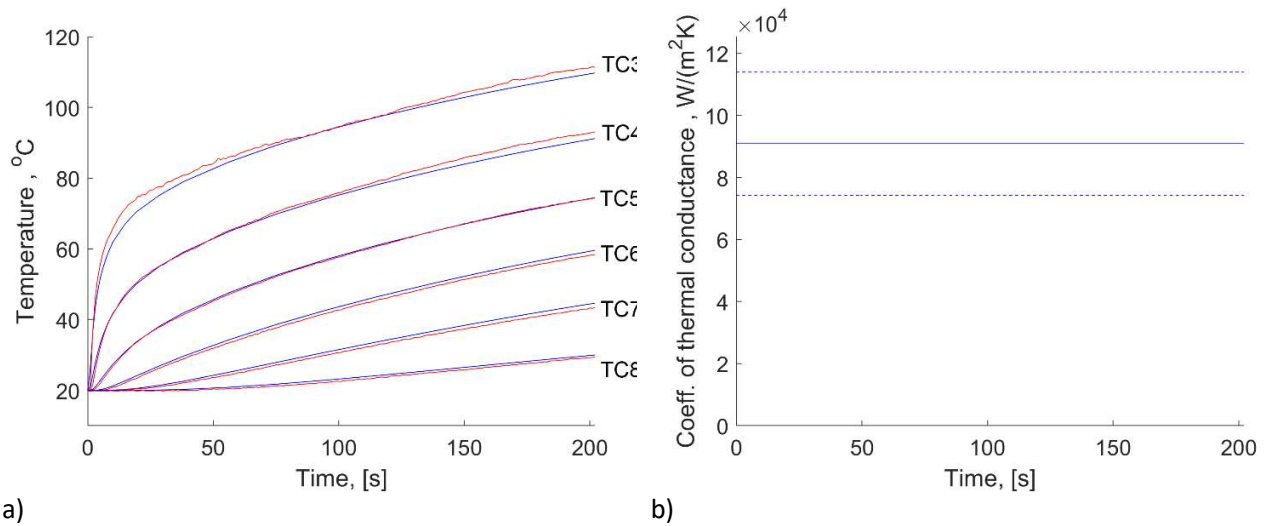

a)
b)
Fig. 10. Results for HSS2. a) Calculated temperatures (blue lines) and measured temperatures (red lines) for the case when the average chip temperature is 406 °C; b) Tool–chip heat exchange coefficient h_{tcc} (solid line) and its uncertainty (dotted lines).

The results of stage 1 for the CC1 case (Table 1) are shown in the Table 3 and Fig. 11.

Table 3. h_{tcc} coefficient returned for the CC1 case.

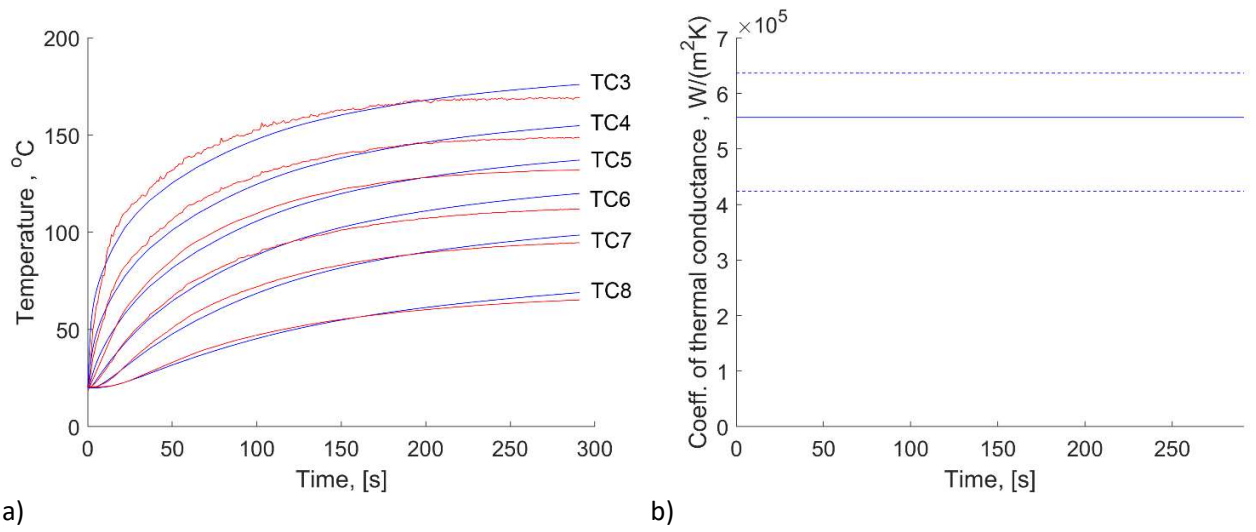| Chip temperature, °C	Coefficient h_{tcc}, W/(m² K)	Objective function, °C
684 (mean)	556957	18.539
714 (upper bound, mean + std. dev.)	423886	19.207
654 (lower bound, mean - std. dev.)	636705	21.337

Fig. 11. Results for HSS2. a) Calculated temperatures (blue lines) and measured temperatures (red lines) for the case when the average chip temperature is 684 °C; b) Tool–chip heat exchange coefficient h_{tcc} (solid line) and its uncertainty (dotted lines).

The very similar values of the objective function for HSS2 and the small differences between calculated and measure temperatures in the first stage show that the calculated h_{tcc} can be used. This is not the case for CC1. The graph for CC1 (Fig. 11a) clearly indicates that the uniform h_{tcc} cannot ensure good agreement between the calculated and measured temperatures. Therefore, it must be considered as a function of time because it is assumed to be spatial uniform across the contact interface. A piecewise line with ten discrete points (Fig. 12) is used as a prototype to model the h_{tcc} time dependency. The values of this function at the points $0, x_1, \ldots, x_9$ are the variables of the objective function in the inverse heat condition problem in stage 2. This parameterization of the function allows us to convert an ill-posed functional problem into a correct parametric function [33].
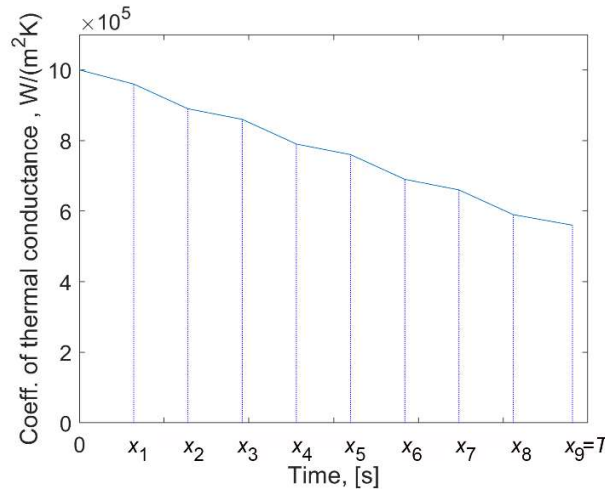

Fig. 12. The parameterized piecewise line for h_{tcc} time dependency modeling.

4.2.2. Results of stage 2

Although the constant h_{tcc} provides reasonable agreement between the measured and calculated temperatures for HSS2, nevertheless for comparison it is useful to calculate h_{tcc} in the form of the function shown in Fig. 12.

Fig. 13 and Fig. 14 illustrate the results of stage 2 for HSS2 and CC1 respectively.
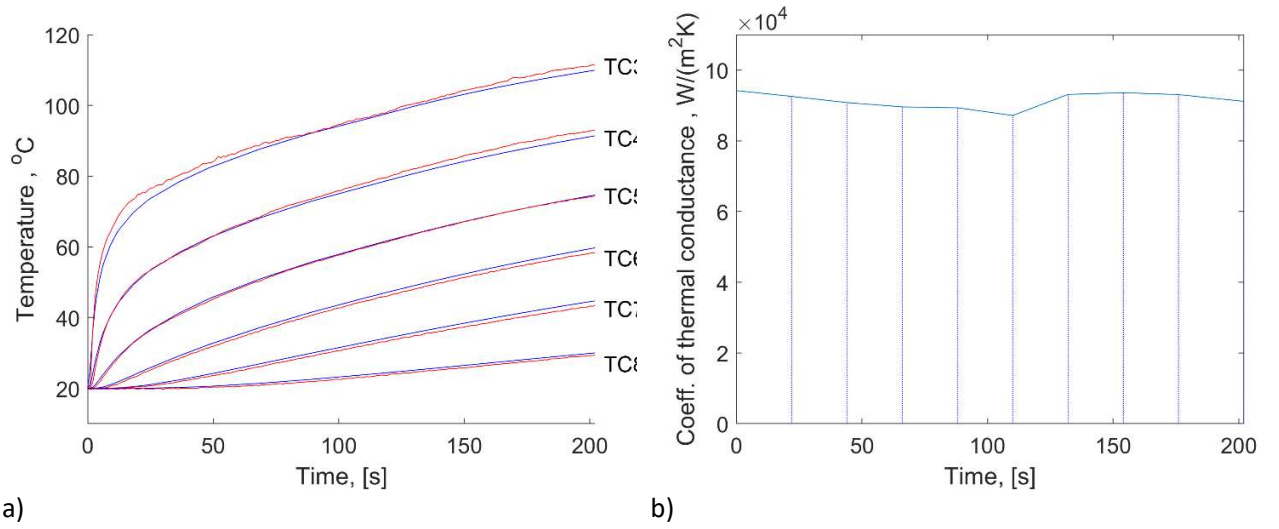
17

Fig. 13. Stage 2 for HSS2. a) Calculated temperatures (blue lines) and measured temperatures (red lines) for the case when the average chip temperature is 406 °C. Objective function $f(h_{tcc}) = 1.338$ °C; b) Time dependency for h_{tcc} obtained for stage 2.
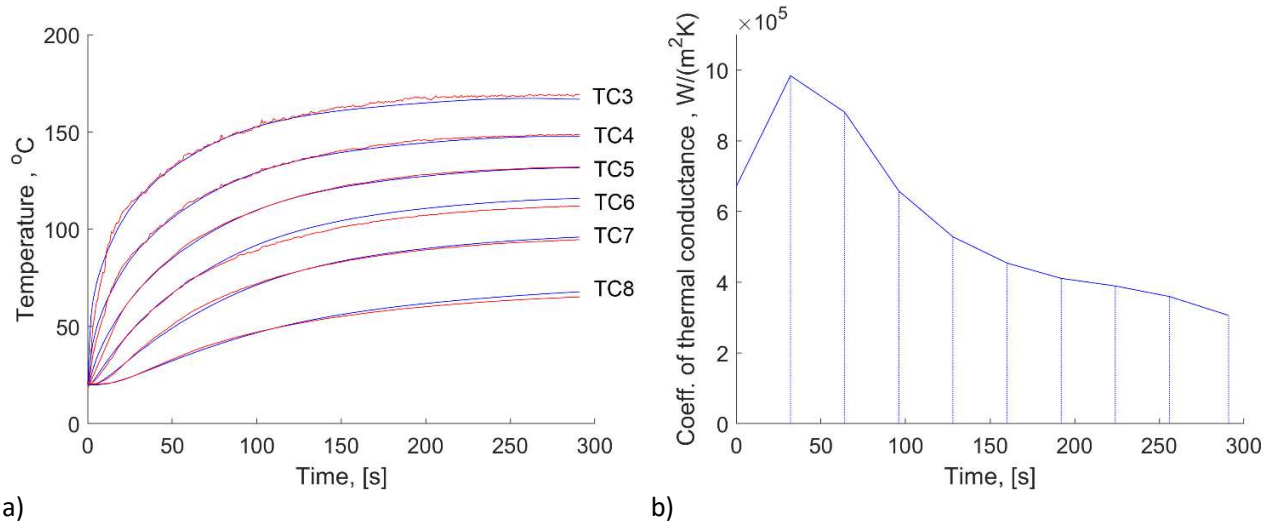

Fig. 14. Stage 2 for CC1. a) Calculated temperatures (blue lines) and measured temperatures (red lines) for the case when the average chip temperature is 684 °C. Objective function $f(h_{tcc}) = 5.178$ °C; b) Time dependency for h_{tcc} obtained for stage 2.

In both cases better agreement between measured and calculated temperatures (Figs. 13a, 14a) and trends in the behavior of h_{tcc} over time (Figs. 13b, 14b) were obtained. In the case of HSS2, h_{tcc} oscillates slightly in stage 2 compared to stage 1 (Fig. 10b vs. 13b). For CC1 there is a pronounced decreasing trend over time of h_{tcc} (Fig. 14b). Traditionally [35–37] a variation in the h_{tcc} coefficient is attributed to a variation in contact pressure or surface topography of the contacting bodies, as these are the two most influential parameters. This will be further investigated in section 6.

5. Time dependency of the heat flux flowing into the tool body

The inverse problem in section 4 allowed us to determine the coefficient $h_{tcc}(t)$ if the average interfacial chip temperature is known. This allowed a numerical solution of the boundary value problem (Eqs. 1, 2, 4, 5). In an implicit form this solution also contains the heat flux from the cutting zone to the tool body. Using the approach used in section 3.3 for the illustrative test case, the same type of data can be extracted for the given machining cases and compared with the heat flux from [21].

To do this, the average heat flux over the region of the tool–chip interface (Fig. 1) as a function of time is calculated in the COMSOL model. This is equivalent to the time-dependent power consumed by the tool. One should take into account that the contact area is also a function of time as described in [21]. The ratio of these two functions determines the function $q(t)$, which describes the heat flux flowing into the tool body for HSS2 (Fig. 15a, blue line) and CC1 (Fig. 15b, blue line).
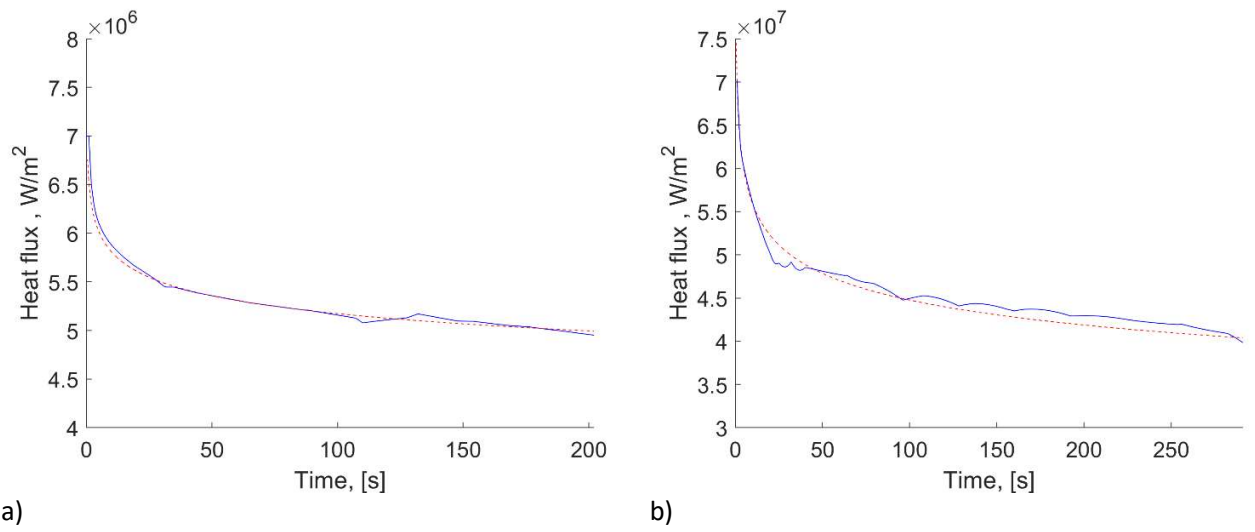

Fig. 15. Comparison of the time dependency of heat flux obtained in the present study (blue) and in [21] (dotted red) for: a) HSS2, b) CC1.

6. The possible form of linkage between micro- and macromodels

Using the experimental setups (section 4.2, [21]), the two-stage technique for solving the inverse heat conduction problem, and macroscopic thermal modeling in COMSOL [21] allowed us to obtain the time-dependent h_{tcc} coefficient for the assumed spatial uniformity across the contact interface. The h_{tcc} value obtained from macroscopic thermal modeling can also be obtained from a microscopic model for contacting bodies [35], thus becoming a transition point for understanding thermal contact from macro- to microscopic perspectives.

Yovanovich's conforming rough surface contact conductance model [35], based on the assumption of a normal distribution of the microcontact spots, has previously been used to model tool–chip contact interaction in machining [38]. The legitimacy of using this model for both sticking and sliding zones assumes that the distribution of the microcontact spots remains normal, although the actual microcontact areas in the sliding zone are changing. In this model h_{tcc} is a function of surface topography and contact pressure:

$$h_{tcc} = \frac{2\,n\,a\,k_{eff}}{\psi(\varepsilon)}. \tag{31}$$

The components of this formula are calculated as follows:

19

$$n \cdot a = \frac{1}{4\sqrt{2\pi}} \left(\frac{m_{eff}}{\sigma_{eff}} \right) exp \left(\frac{-\lambda^2}{2} \right), \tag{32}$$

$$\psi(\varepsilon) = (1 - \varepsilon)^{1.5}, 0 < \varepsilon < 0.3, \tag{33}$$

$$\varepsilon = \sqrt{\frac{P}{H_C}}, \tag{34}$$

where $\lambda = \frac{Y}{\sigma}$ is the relative mean plane separation, Y is the distance between the mean planes of the contacting surfaces, $k_{eff}, m_{eff}, \sigma_{eff}$ are the effective thermal conductivity, slope and RMS surface roughness of the contacting bodies, respectively.

The effective parameters $k_{eff}, m_{eff}, \sigma_{eff}$ are given by:

$$k_{eff} = \frac{2k_1 k_2}{k_1 + k_2}, m_{eff} = \sqrt{m_1^2 + m_2^2}, \sigma_{eff} = \sqrt{\sigma_1^2 + \sigma_2^2}, \tag{35}$$

where k_1, m_1, σ_1 and k_2, m_2, σ_2 are corresponding parameters of the contacting bodies.

In this formulation the product $n \cdot a$ relates to topography, while ε is solely dependent on the ratio "pressure-microhardness" (Eq. 34). Thus Eq. 31 for h_{tcc} has two unknown input components, neither of which can be explicitly extracted from it. To resolve this, the model (Eq. 31) needs to be complemented with additional experimental data to remove ambiguity. Measuring the cutting forces and the time-dependent data of the contact area [21] provides information on the time-dependent average contact pressure (Fig. 16).
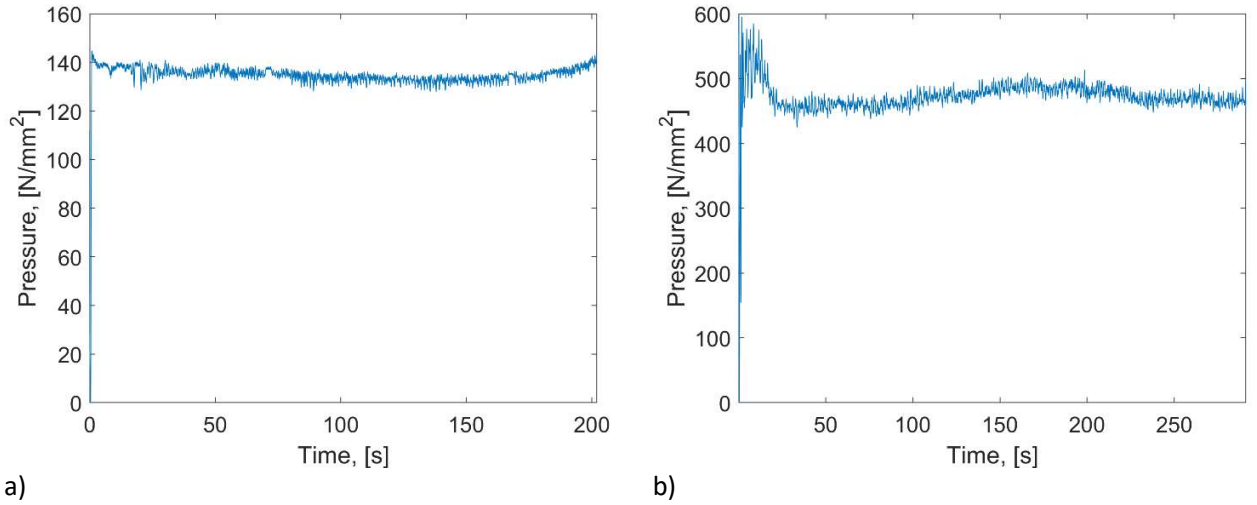

Fig. 16. The average contact pressure for: a) HSS1, b) CC1.

Fig. 16a and Fig. 16b for HSS2 and CC1 indicate that practically constant contact pressure is maintained during the entire machining operation, compared to the behavior of h_{tcc} (Fig. 13b and Fig. 14b). Thus the "pressure-microhardness" ratio is practically constant as well. However, the value of the contact microhardness H_C assigned to the deformation of the contacting asperities is unknown. Therefore, to estimate the ratio in Eq. 34, the following formula can be used [35]:

$$\frac{P}{H_C} = \frac{1}{2} erfc \left(\frac{\lambda}{\sqrt{2}} \right). \tag{36}$$

The surface topography component has an additional complexity as it includes the initial surface topography of the two bodies not yet in contact, and geometric parameters Y of topography interaction under the actual machining conditions.

The original (not in contact) topography was measured on the cutting tools before and after machining, as well as on back side of the chips collected at the beginning and end of the cut. Table 4 indicates the topography of tool surfaces, characterized in terms of RMS surface roughness and slope, measured at 200 cross-sections for each data set (Fig. 17). For HSS2 the values remain practically unchanged, while for the CC1 case a substantial increase in roughness is observed for the tool after machining. Chip roughness parameters at the beginning and end of cutting were practically identical.

Table 4. Tool and chip roughness parameters.

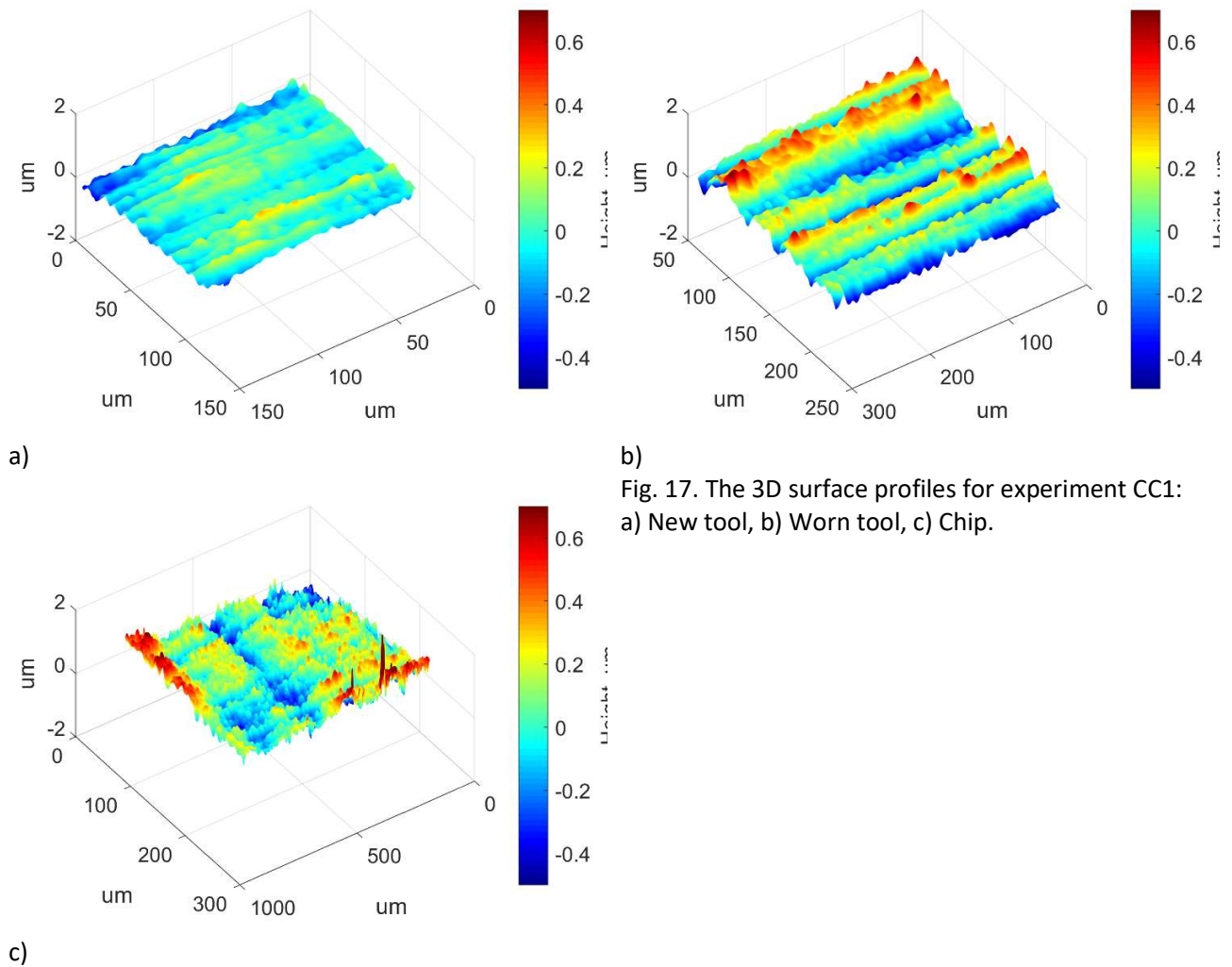| Experiment acronym	Tool before test		Tool after test		Chip	
	RMS, um	Slope	RMS, um	Slope	RMS, um	Slope
HSS2	0.097	0.016	0.106	0.016	0.126	0.018
CC1	0.0946	0.014	0.3	0.015	0.186	0.02

a)

b)

Fig. 17. The 3D surface profiles for experiment CC1: a) New tool, b) Worn tool, c) Chip.

c)

Then, having a linear approximation of effective RMS roughness and slope over the experiment time, Y can be calculated from the model (Eqs.31–34) for HSS2 (Fig. 18a) and CC1 (Fig. 18b).
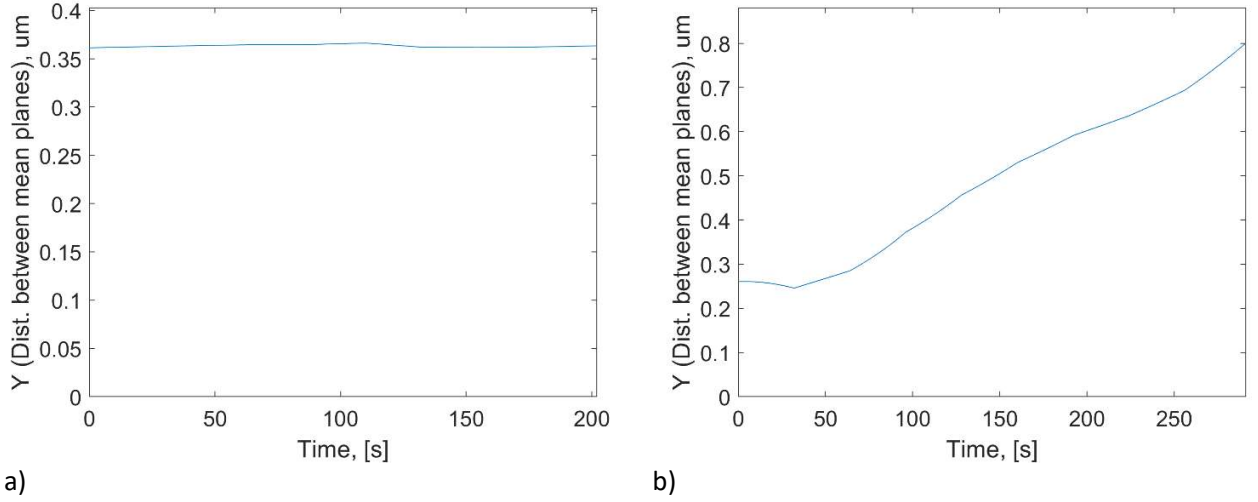

Fig. 18. Distance Y between the mean planes of the contacting surfaces for a) HSS2, b) CC1.

These data indicate that geometric parameter Y of the interaction between tool and chip topographies under the actual machining conditions remains stable throughout the HSS2 experiment. Y increases for the CC1 test, which is related to workpiece adhesion and tool wear [21]. Thus macroscopic modeling of h_{tcc} allowed estimating the in-process interaction parameter Y, which cannot be measured otherwise. There is additional value from the modeling, as h_{tcc} is actually the inverse of the thermal resistance of the chip-tool contact, which is frequently used in FE modeling of machining operations.

7. Conclusions

This study presents qualitative and quantitative research on the role of the tool–chip thermal conductance coefficient h_{tcc} for modeling the heat flux transferred into the tool body when machining.

1. A qualitative analysis of the mixed boundary condition for the heat equation showed that the heat flux into the tool body is a decreasing function over time if the average chip temperature and the tool–chip thermal conductance coefficient h_{tcc} do not vary with time. This consideration also demonstrates that the heat flux depends parametrically on the average interfacial chip temperature u_{chip} and the tool–chip thermal conductance coefficient h_{tcc}. Thus these two parameters are considered to be the variables of the inverse heat conduction problem.

2. A qualitative analysis of an illustrative test case shows that solving the inverse problem requires determining the average interfacial chip temperature. If u_{chip} and h_{tcc} are considered as two independent variables, an optimization algorithm creates a compensation effect between them, and the inverse heat transfer problem cannot be solved effectively. An experimental setup was designed, and experiments were performed to determine average chip temperature for two pairs of tool–workpiece materials. This allowed one variable to be excluded from the inverse problem solution, leaving only the tool–chip thermal conductance coefficient as a variable.

3. A two-stage method was used to solve the inverse problem. For both tests, the tool–chip thermal conductance coefficients are obtained as time-dependent functions. As soon as the coefficients are known, a technique for numerical identification of the heat flux into the tool is demonstrated. Also, it is shown (section 5) that the heat flux time dependency can be approximated by a decreasing power function.

4. An estimate of the in-process tool–chip contact characteristics on the microscale is obtained using the tool–chip thermal conductance coefficient and the conforming rough surface contact conductance model. It was shown that time dependency of h_{tcc} is governed by a change in tool surface topography as the tool wears.

Because the inverse heat condition problem is ill-posed, the reconstruction of the temperature distribution in a tool body using inverse techniques is rooted in the absence of reliable a priori information about the solution behavior. This paper established that, in the class of problems under consideration, the time dependency of the heat flux must be chosen only from the set of decreasing (non-increasing) functions. A suitable approximation can be a power function depending on coefficient h_{tcc}, for which a reliable solver has been developed. Subsequently, h_{tcc} is used as a parameter for transition from macro- to microscale modeling evolution of the tool–chip contact over time. If spatial information is available for the heat flux, this approach can be expanded to estimate thermal contact and tool–chip contact parameters in space, that is, across the tool–chip interface.

References

[1] M.A. Davies, T. Ueda, R. M'Saoubi, B. Mullany, A. L. Cooke, On the measurement of temperature in material removal processes, Annals of the CIRP 56(2) (2007) 581–604.

[2] P.J. Arrazola, T. Ozel, D. Umbrello, M. Davies, I.S. Jawahir, Recent advances in modelling of metal machining processes, CIRP Annals – Manufacturing Technology 62 (2013) 695–718.

[3] J. Ji, Y. Huang, K.-M. Lee, Cutting tool temperature field reconstruction using hybrid macro/micro scale modeling for machining of titanium alloy, IEEE Int. Conf. on Adv. Intelligent Mechatronics (AIM) (2016).

[4] J.-E. Ståhl, Metal Cutting: Theories and Models. Fagersta: SECO Tools, (2012).

[5] T. Jin, D.J. Stephenson, Heat flux distributions and convective heat transfer in deep grinding, International Journal of Machine Tools & Manufacture 46 (2006) 1862–1868.

[6] C.-H. Huang, Hung-Chi Lo, A three-dimensional inverse problem in predicting the heat fluxes distribution in the cutting tools, Numerical Heat Transfer Part A 48 (2005) 1009–1034.

[7] J.-L. Battaglia, A. Kusiak, Estimation of heat fluxes during high-speed drilling, Int J Adv Manuf Technol 26 (2005) 750–758.

[8] M. Putz, G. Schmidt, U. Semmler, Ch. Oppermann, M. Bräunig, U. Karagüzel, Modeling of heat fluxes during machining and their effects on thermal deformation of the cutting tool, Procedia CIRP 46 (2016) 611–614.

[9] G. List, D. Géhin, A. Kusiak, J.L. Battaglia, F. Girot, Heat flux and temperature at the tool–chip interface in dry machining of aeronautic aluminium alloy, Heat Flux: Processes, Measurement Techniques and Applications (2011) 197–210.

[10] S. Han, P. Faverjon, F. Valiorgue, R. Joël, Heat flux density distribution differences in four machining processes of AlSi7 block: MQL drilling, tapping, reaming and dry milling, Procedia CIRP 58 (2017) 61 – 66.

[11] H. R.B. Orlande, O. Fudym, D. Maillet, R.M. Cotta, Thermal Measurements and Inverse Techinques, CRC Press, Taylor & Francis Group (2011).

[12] J.-L. Battaglia, A modal approach to solve inverse heat conduction problems, Inverse Problems in Engineering 10(1) (2002) 41–63.

[13] V. Norouzifard, M. Hamedi, A three-dimensional heat conduction inverse procedure to investigate tool–chip thermal interaction in machining process, Int J Adv Manuf Technol 74 (2014) 1637–1648.

[14] R.F. Brito, S.R. Carvalho, S.M.M. Lima E Silva, Experimental investigation of thermal aspects in a cutting tool using comsol and inverse problem, Applied Thermal Engineering 86 (2015) 60–68.

[15] S. Huang, B. Tao, J. Li, Y. Fan, Z. Yin, Estimation of the time and space-dependent heat flux distribution at the tool–chip interface during turning using an inverse method and thin film thermocouples measurement, Int J Adv Manuf Technol 99 (5–8) (2018) 1531–1543.

[16] V. Kryzhanivskyy, V. Bushlya, O. Gutnichenko, R. M'Saoubi, J.-E. Ståhl, Influence of tool material and tool wear on tool temperature in hard turning reconstructed via inverse problem solution, Journal of Superhard Materials 39(3) (2017) 192–202.

[17] V. Kryzhanivskyy, V. Bushlya, O. Gutnichenko, R. M'Saoubi, J.-E. Ståhl, Computational and experimental inverse problem approach for determination of time dependency of heat flux in metal cutting, Procedia CIRP 58 (2017) 122–127.

[18] H.-J. Kim, N.-K. Kim, J.-S. Kwak, Heat flux distribution model by sequential algorithm of inverse heat transfer for determining workpiece temperature in creep feed grinding, International Journal of Machine Tools & Manufacture 46 (2006) 2086–2093.

[19] P. Kwon, T. Schiemann, R. Kountanya, An inverse estimation scheme to measure steady-state tool–chip interface temperatures using an infrared camera, International Journal of Machine Tools & Manufacture 41 (2001) 1015–1030.

[20] B. Wei, G. Tan, N. Yin, L. Gao, G. Li, Research on inverse problems of heat flux and simulation of transient temperature field in high-speed milling, Int J Adv Manuf Technol 84 (2016) 2067–2078.

[21] V. Kryzhanivskyy, V. Bushlya, O. Gutnichenko, R. M'Saoubi, J.-E. Ståhl, Heat flux in metal cutting: Experiment, model, and comparative analysis, International Journal of Machine Tools and Manufacture 134 (2018) 81–97.

[22] J.V. Beck, B. Blackwell, Ch. R. St. Clair Jr. Inverse Heat Conduction: Ill-Posed Problems, New-York: A Wiley-Interscience Publication (1985).

[23] A. N. Tikhonov, V. Y. Arsenin, Solution of Ill-posed Problems. Washington: Winston & Sons (1977).

[24] G. Dour, M. Dargusch, C. Davidson, Recommendations and guidelines for the performance of accurate heat transfer measurements in rapid forming processes, International Journal of Heat and Mass Transfer 49 (2006) 1773–1789.

[25] V.S. Vladimirov, Equations of Mathematical Physics, M. Dekker, New York (1971) 418.

[26] V. Norouzifard, M. Hamedi, Experimental determination of the tool–chip thermal contact conductance in machining process, International Journal of Machine Tools & Manufacture 84 (2014) 45–57.

[27] J. Rech, P.J. Arrazola, C. Claudin, C. Courbon, F. Pusavec, J. Kopac, Characterisation of friction and heat partition coefficients at the tool-work material interface in cutting, CIRP Annals - Manufacturing Technology 62 (2013) 79–82.

[28] C. Courbon, T. Mabrouki, J. Rech, D. Mazuyer, E. D'Eramo, On the existence of a thermal contact resistance at the tool-chip interface in dry cutting of AISI 1045: Formation mechanisms and influence on the cutting process, Applied Thermal Engineering 50 (2013) 1311-1325.

[29] A. K. Balaji, G. Sreeram, I. S. Jawahir, E. Lenz, The effects of cutting tool thermal conductivity on tool-chip contact length and cyclic chip formation in machining with grooved tools, CIRP Annals - Manufacturing Technology 48 (1) (1999) 33–38.

[30] Y. Avevor, A. Moufki , M. Nouari, Analysis of the frictional heat partition in sticking-sliding contact for dry machining: an Analytical-Numerical modelling, Procedia CIRP 58 (2017) 539–542.

[31] C.V. Pao, Nonlinear Parabolic and Elliptic Equations, Springer Science & Business Media (1992).

[32] D. V. Schroeder, An Introduction to Thermal Physics, Addison Wesley (2000).

[33] K. Woodbury, Inverse Engineering Handbook, CRC Press, Boca Raton (2002).

[34] R. M'Saoubi, H. Chandrasekaran, Investigation of the effects of tool microgeometry and coating on tool temperature during orthogonal turning of quenched and tempered steel, International Journal of Machine Tools and Manufacture 2-3 (44) (2007) 213–224.

[35] M. M. Yovanovich, Four decades of research on thermal contact, gap, and joint resistance in microelectronics, IEEE transactions on components and packaging technologies 28(2) (2005) 182–206.

[36] C. V. Madhusudana, Thermal Contact Conductance, Springer (1996).

[37] S. Kumar, A. Tariq, Determination of thermal contact conductance of flat and curvilinear contacts by transient approach, Experimental Thermal and Fluid Science 88 (2017) 261–276.

[38] M.H. Attia, L. Kops, A new approach to cutting temperature prediction considering the thermal constriction phenomenon in multi-layer coated tools, CIRP Annals - Manufacturing Technology 53(1) (2004) 47–52.

[39] https://www.engineeringtoolbox.com/radiation-heat-emissivity-aluminum-d_433.html.